A preliminary investigation on the use of the pin-on-disc test to simulate off-brake friction and wear characteristics of friction materials

Matteo Federici[1], Stefano Gialanella[1], Mara Leonardi[1], Guido Perricone[2], Giovanni Straffelini[1*].

[1]Dept. of Industrial Engineering, University of Trento, Via Sommarive 9, Povo, Trento, Italy

[2] Brembo S.p.A, Stezzano, Bergamo, Italy

*Corresponding author

ABSTRACT

During off-brake driving, some unwanted contact between the brake pads and the rotating discs may occur, thus inducing inefficient fuel usage and additional environmental pollution. This paper addresses the frictional behavior of 5 commercial low-met and NAO friction materials dry sliding against a cast iron counterface disc, under low contact pressures, typical of off-brake driving. In the investigated conditions, kinetic and static coefficient of frictions (COFs) were found to be independent from the contact pressure. The static COFs were all found to be around 0.2, whereas the kinetic COFs were found to be higher in the low-met materials with respect to the NAO materials and they were found to be roughly independent from the contact pressure. The results were explained with reference to the adhesive theory of friction, highlighting the paramount role of the Fe-oxides embedded in the friction layer.

Keywords:

Automotive brakes; Off-brake conditions; Contact pressure; Friction materials; Transfer layer; Pin-on-disc testing.

1. Introduction

In automotive braking systems, the friction forces between stationary pads and a rotating disc allows the vehicle to stop. Friction also induces an energy dissipation, associated with a material wearing out, that results in a thermal load on the brake parts and emission of wear particles in the environment [1, 2]. Even during off-brake conditions some unwanted contact between the pads and the disc may occur, because of the imperfect alignment between the disc and the pad, disc distortions, or an imperfect caliper operation. Therefore, frictional energy may be also dissipated in off-brake conditions, and this contributes further not only to the emission of wear particles but also to a less efficient engine combustion, with increased CO_2 emissions. It is reported that 1Nm drag torque at each wheel may induce an emission of 2 grams CO_2 per km [3]. It would be clearly preferable to have friction couplings capable to guarantee a relatively high Coefficient of Friction (COF) during normal braking conditions, i.e., a COF in the range 0.3-0.6, and a lower COF in off-brake conditions, when the contact pressure is low, below 50 kPa [3], to be compared with pressures in the 1-3 MPa range for conventional braking.

Nowadays, rotor discs for vehicular brakes are typically made of pearlitic cast iron and pad materials are composites, containing even more than 30 ingredients, and often classified as low-metallic (low-met) and Non Asbestos Organic (NAO) materials [4, 5]. Several investigations have demonstrated that the COF and system wear depend on the characteristics of the friction layer that forms at the pad-disc contact region, which in turn depends on the composition and characteristics of the mating materials. The friction layer is made of primary and secondary plateaus (called also 'patches') [6-9]. Primary plateaus consist of hard particles and fibers, even metallic, protruding from the pad surface. Secondary plateaus are made of wear debris that pile up and are compacted against the primary plateaus. The specific features of the friction layer determine the frictional and the wear behavior of the sliding system, since such plateaus are responsible for the transmission of the friction force from the pad to the disc [6, 10]. In general, at the beginning of sliding, a run-in stage is required to form an effective friction layer [11]. During this stage, wear debris result from the wear of the pad and the possible fragmentation of the friction layer, together with the abrasive and tribo-oxidative wearing out of the cast iron disc. This latter mechanism results in the formation of small iron oxides, typically magnetite and hematite [12], particles. Such smaller debris are able to pile-up and form the main components of well compacted secondary plateaus, a prerequisite for a smooth and stable COF. On the other hand, less compacted secondary plateaus generally determine an evolution of the coefficient of friction characterized by a larger scatter, because of the dynamic fragmentation and reformation of the contacting plateaus [9]. The presence in the friction material of such elements as copper, graphite, and other soft components, like metal sulfides, promote the formation of well compacted secondary plateaus [12]. A recent investigation by Lee and Filip [13], has confirmed further these observations with reference to the friction and wear behavior of different NAO materials. In the case of the friction materials containing Cu, barite and other ingredients, particularly prone to adhere with each other, a stable friction layer was obtained during sliding and a lower level of friction and wear was detected. In different investigations [12, 14, 15], Österle and coworkers also showed the paramount role played of solid lubricants, such as graphite, in the compaction of iron oxide, namely magnetite (Fe_3O_4), particles to form dense secondary plateaus. Of course, because of the presence of different ingredients in the secondary plateaus, the values of the friction coefficient were found to be lower than 0.8, a typical reference value exhibited by the steel-steel contact under tribo-oxidative conditions [12, 16].

In the present work, we investigated the friction behavior of five commercial friction materials, sliding against a pearlitic cast iron. The kinetic COF was measured using a Pin-on-Disc (PoD) test rig, operating in drag conditions and at nominal contact pressures between 15 and 50 kPa. To help explaining the obtained results, specific wear tests were also conducted for evaluating the static friction coefficient in the same contact conditions [17]. The aim of the investigation was to determine the friction behavior of typical low-met and NAO brake materials at low contact pressures and to relate the results to the

characterization of the friction layer, in particular the secondary plateaus in order to explore the possibility to obtain low values of the COF at low contact pressures.

2. Materials and experimental procedures

2.1 Friction materials

Five different commercial friction materials were investigated. Their elemental composition, as measured by energy dispersive X-ray spectroscopy (EDXS), is reported in Table 1. As a rule of thumb, low-met materials usually contain a total amount of metallic Fe and Cu in the range 10-50 wt.%; NAO materials contain a lower amount of metallic ingredients, typically below 10 wt.%. The classification is also based on the average values of the COF, since low-met materials would generally feature comparatively high COF, usually in between 0.4 and 0.6, when sliding against pearlitic cast iron discs. NAO materials exhibit lower COFs, usually not exceeding 0.4 [5]. The comparative indications provided by the EDXS results in Table 1 show that the friction materials 1 and 2 can be classified as low-met, whereas material 5 is a NAO. Material 3 and 4 are in between. Considering that in general NAO materials display a lower friction coefficient with respect to low-met materials and on the basis of the results reported later on this work, we can consider material 3 and 4 as NAO.

Element	**Friction material 1 [wt.%]**	**Friction material 2 [wt.%]**	**Friction material 3 [wt.%]**	**Friction material 4 [wt.%]**	**Friction material 5 [wt.%]**
Fe	15.8	26.6	21.2	12.4	0.7
Al	10.3	17.8	13.8	5.6	1.3
Mg	11.5	12.2	13.6	1.0	7.4
Cu	13.7	11.3	-	11.0	-
Sn	9.4	8.0	7.2	4.0	3.0
Zn	15.8	6.8	14.9	3.5	-
Ca	7.6	5.9	5.7	2.5	5.0
S	4.9	4.7	9.3	3.3	4.2
Cr	3.1	3.1	4.0	-	-
Si	6.8	3.1	7.4	3.1	4.2
K	-	0.5	-	3.3	6.1
Na	1.1	-	2.9	5.6	1.3
Zr	-	-	-	27.3	30.6
Ti	-	-	-	14.0	27.6
Ba	-	-	-	3.4	6.8
F	-	-	-	-	1.8

Table 1: Elemental composition of the friction materials investigated in the present study (the concentrations of C and O are not included in the table).

Fig. 1 shows the SEM micrographs of the five friction materials. From the EDXS maps, not included in the present report, the main ingredients have been identified, as indicated in the relevant SEM micrographs. Material 5 is characterized by a fine homogeneous distribution of the constituent phases. All other materials feature a rather inhomogeneous microstructure, containing comparatively coarser ingredients, including metallic fibers or powders, coke particles and abrasives, such as MgO (in friction materials 1,2 and 3), alumina (materials 1,3 and 4) and zirconia (material 4).

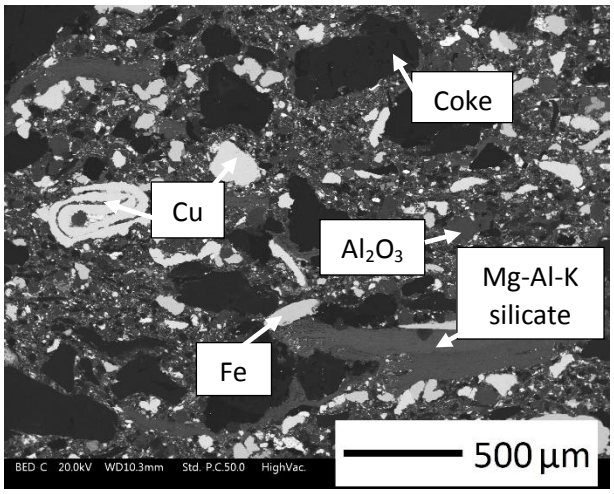

(a)

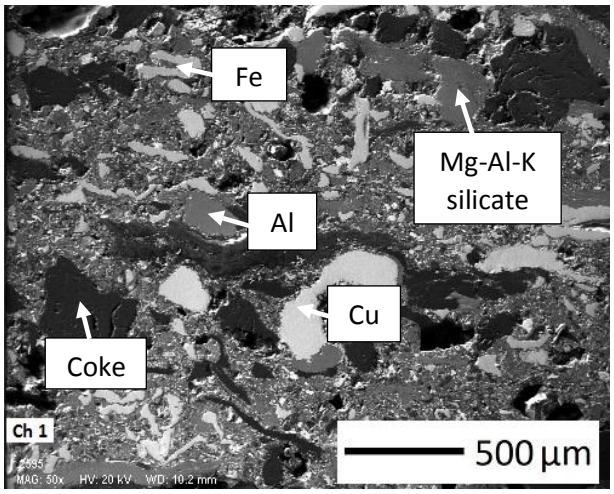

(b)

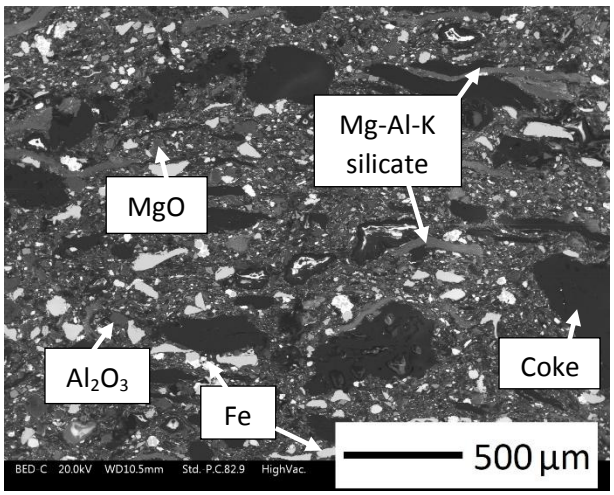

(c)

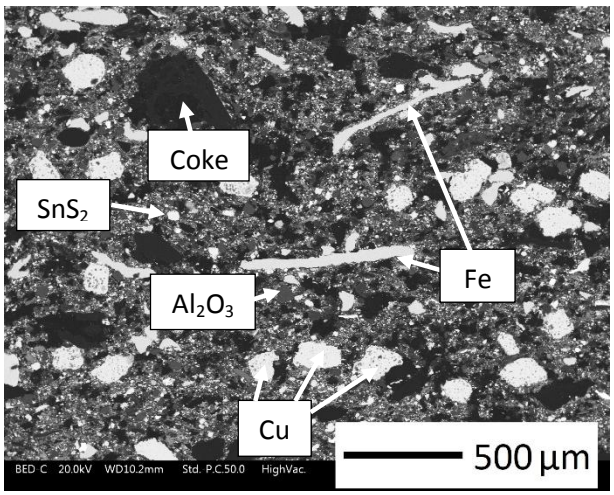

(d)

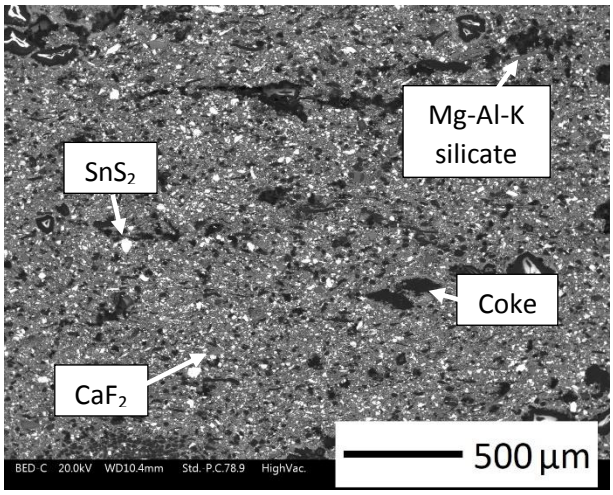

(e)

Fig.1: SEM micrographs of the friction materials: a) to e) corresponding to material 1 to material 5 (see table 1).

2.2 Experimental procedure

The sliding tests, aimed at obtaining the evolution of the kinetic COF, were performed in dry sliding conditions by means of an Eyre/Biceri PoD test rig. The pins had cylindrical shapes and they were machined from commercial brake pads. The diameter of the pins was of 30 mm and the height of 15 mm. The discs are made of a pearlitic gray cast iron with a hardness of 209 ± 3 HV30. The discs were 140 mm in diameter and 15 mm in height.

The materials were tested at room temperature and at a nominal contact pressure of 15, 30 and 50 kPa (the load was applied using a dead weight). The sliding velocity was 2.88 m/s in all cases, and the test duration was 1 hour. Before each test, a preliminary running-in stage was performed at 200 kPa in order to establish a proper friction layer on the pin surface in a relatively short time (1.5 hours). In any case, the parallelism between the PoD arm and the rotating disc was checked before and after each test. During the entire test the COF was continuously recorded. The results presented are the average of at least three different repetitions. Pin wear was also measured by checking its weight before and after each test using an analytical balance with a precision of 10^{-4} g. Data were then converted into wear volumes and the specific wear coefficients, Ka, were calculated by dividing the volume loss for the applied load and sliding distance. The worn surfaces of pins were analyzed by means of JEOL IT300 scanning electron microscope (SEM) equipped with an EDXS system. The worn out surfaces of the discs were observed by means of an optical microscope (OM).

The static COF, using both run-in tested and pins and discs in their pristine conditions, was measured by means of the experimental apparatus schematized in Fig. 2. In the case of preliminarily PoD tested pins, the same couple used during the wear tests was used. To avoid any possible indeterminations in the actual pressure, due to different contact times between pins and discs, all the tests were performed after 10 seconds of pin-disc contact [17]. The velocity of the dynamometer was set equal to 0.1 cm/s. The results of these tests are the average of five different measurements for each material.

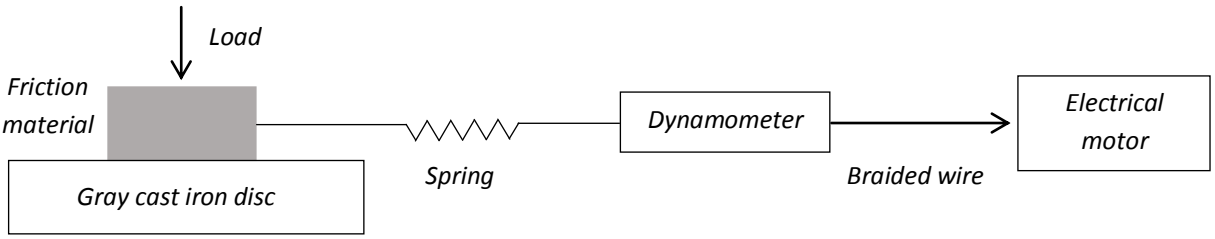

Fig. 2: Schematic of the experimental set-up for the measurements of the static friction coefficients.

3. Results

As an example, the top view of the worn out surfaces of the pins of the materials 1 and 4 after the running-in stage PoD tests, conducted at 200 kPa are shown in Fig. 3: well compacted and widely distributed plateaus are visible. The same was observed in the other materials tested at 200 kPa.

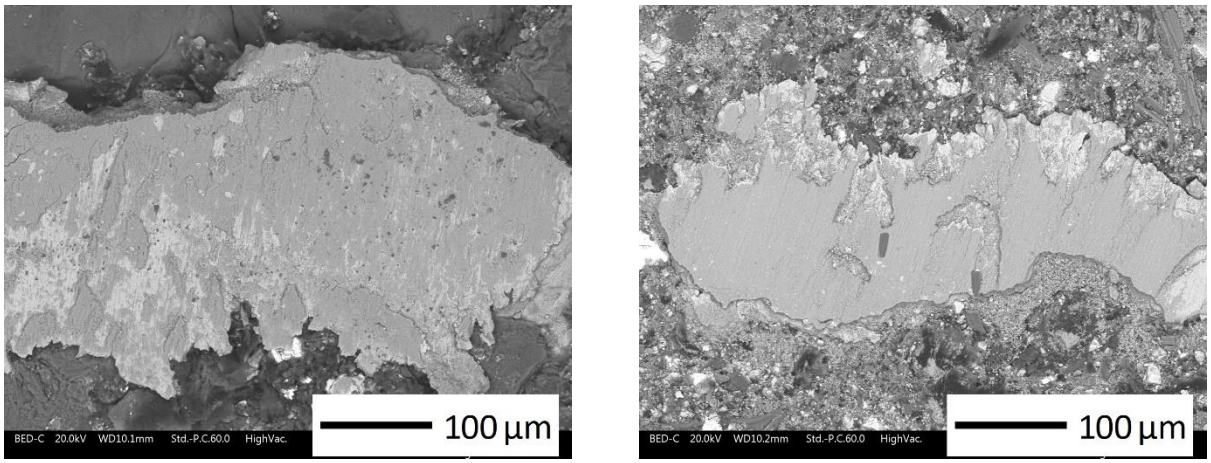

(a) (b)

Fig.3: SEM micrographs of the sliding surfaces of the Friction material 1 (a) and 4 (d) after the running-in procedure in PoD tests conducted at an applied pressure of 200 kPa.

The evolution of the COFs is shown in Fig. 4 for the friction materials 1 and 4. The curve for material 1 is representative of the COF evolution displayed also by the friction materials 2 and 3. The evolution of the COF for material 4 is similar to the evolution observed with material 5. It can be seen that, the low-met material 1 showed a much longer running-in stage (approximately 1500 s vs. 200 s), and, afterward, a higher steady-state friction coefficient with respect to material 4. The experimental steady-state kinetic COFs are then displayed in Fig. 5. It can be seen that materials 1 and 2 display higher COFs as compared to the other three friction materials. It can be concluded that materials 1 and 2 behave like typical low-met materials, whereas materials 3, 4 and 5 behave all like NAO materials, even if the total metallic content of material 3 is 21.2% (Table 1). Most importantly, it can be seen that COF is independent from the contact pressure, and therefore it does not decrease upon reducing the applied pressure, as it would have been desired.

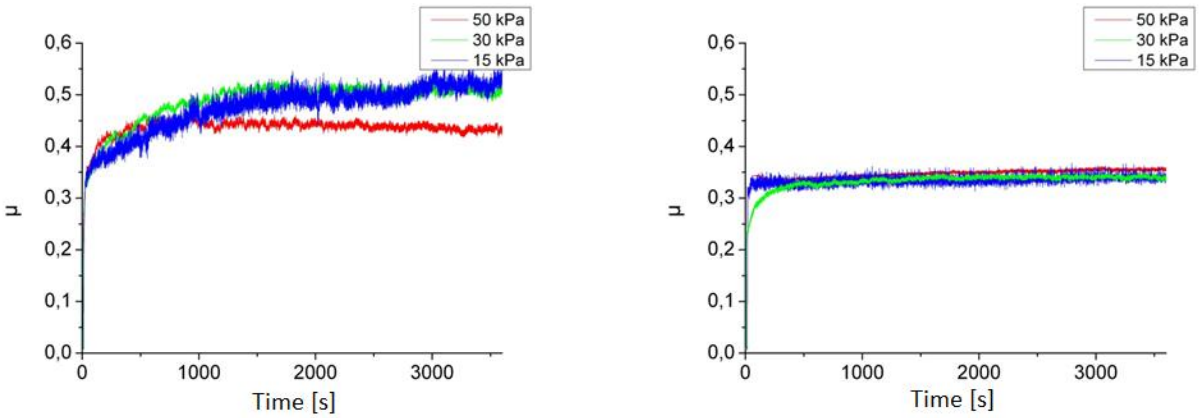

(a) (b)

Fig. 4: Evolution of the friction coefficient during the PoD tests for the friction material 1 (a) and 4 (b), conducted at the pressures indicated in the graphs.

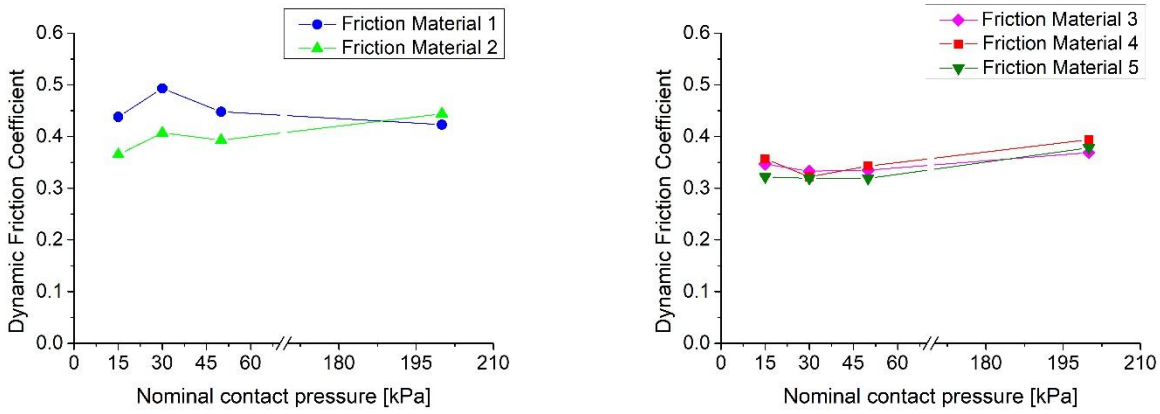

(a) (b)

Fig.5: Steady state friction coefficients for the low-met (a) and NAO (b) friction materials.

Fig. 6 depicts the specific wear coefficients of low-met (a) and NAO (b) friction materials. In agreement with the values of the dynamic COF, the specific wear coefficients of the low-met materials are higher than those of the NAO materials.

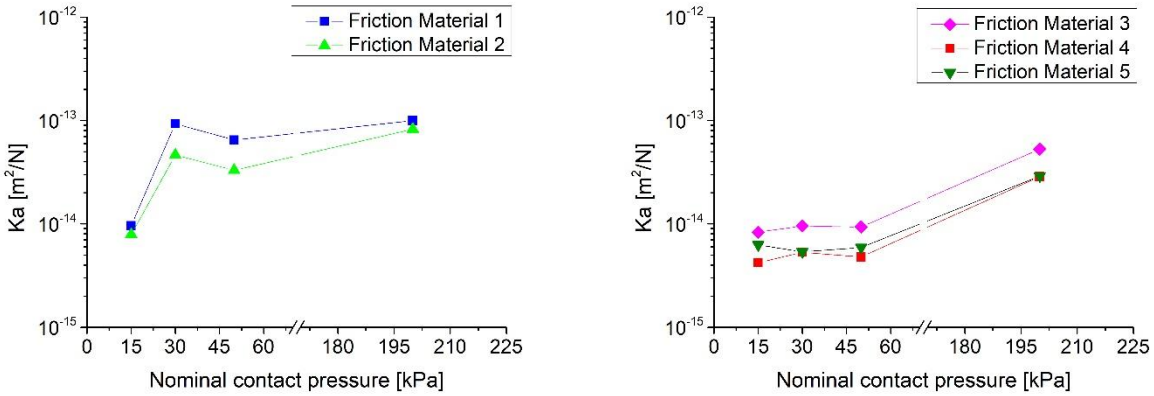

(a) (b)

Fig. 6: Specific wear coefficients of low-met (a) and NAO (b) friction materials.

Fig. 7 shows the top views of the worn out pins, friction materials 1 and 4, tested at 15, 30 and 50 kPa. As expected, primary and secondary plateaus can be observed in the friction layers present on the pin surface. The EDXS analyses showed that the primary plateaus are mainly constituted of Fe and Cu fibers, for the low-met materials. In the case of NAO materials, the primary plateaus are mostly made of large ceramic particles, such as ZrO_2 and Mg-K-silicate particles. Table 2 shows the results of the chemical analyses of the secondary plateaus for the samples tested at 30 kPa. The tests conducted at the other different contact pressures provided similar results. From a comparison of the compositional data in Table 2 with those in Table 1 emerges that all the ingredients of the friction materials are present in the relevant secondary plateaus that are formed on the pin surface. Iron, originating from the wear of the disc counterface, is also present, in larger amount in the case of the low-met materials, and in lower amount in the case of NAO materials (in particular material 4), coherently with the lower recorded values of the relevant COF.

Fig.8 shows the top views of the worn surfaces of the discs after sliding against materials 1 and 4 at 30 kPa applied pressure. In the first case, the presence of abrasive grooves in the direction of sliding can be appreciated. These grooves appear alternatively white and grey. The white grooves are exposing the metallic matrix of the cast iron disc. The grey regions and grooves are covered either by transferred particles from the friction layer or by native oxides resulting from the tribo-oxidative wear of the cast iron disc, according to literature reports [18-20]. Regions where the graphite flakes reach the disc surface can be also observed (see the arrowed regions in Fig. 8). In case of the disc worn against friction material 5 (Fig, 8b), the damage features are similar to those observed in case of material 1, with the additional presence of some patches of compacted wear debris back-transferred from the pin surface (see arrows and labels in Fig. 8b).

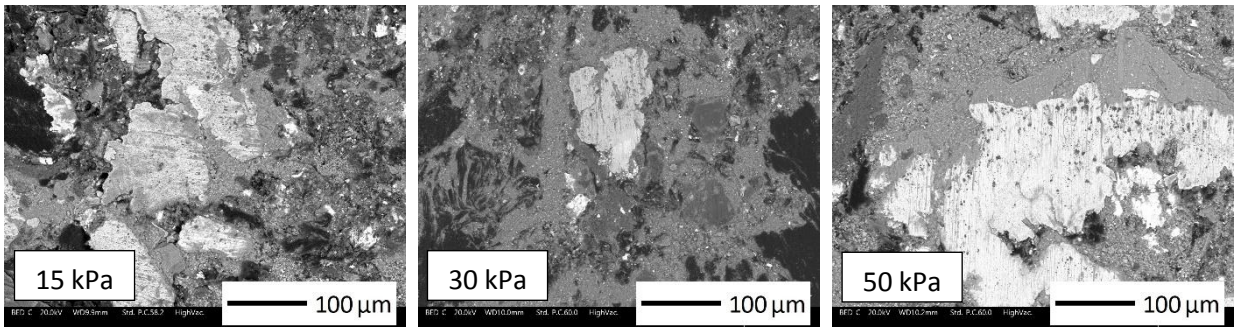

(a)

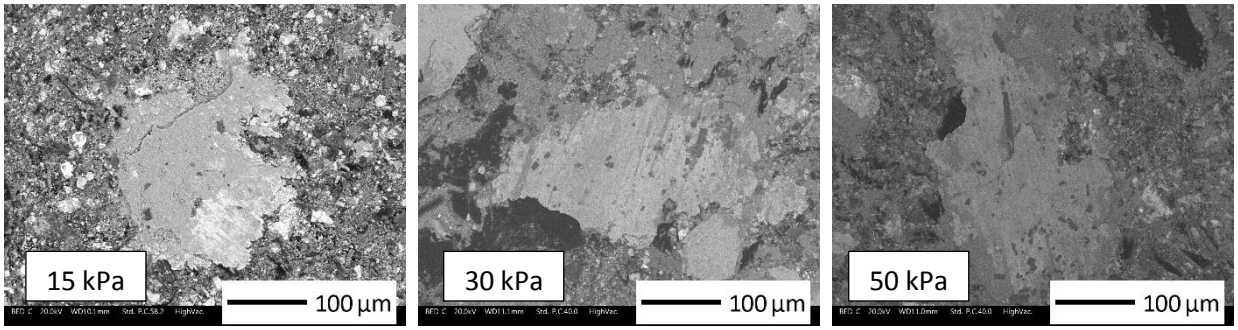

(b)

Fig. 7: Top view of the worn surfaces of the pin made of material 1 (a) and 4 (b) tested at different pressures, as indicated in the relevant SEM micrographs.

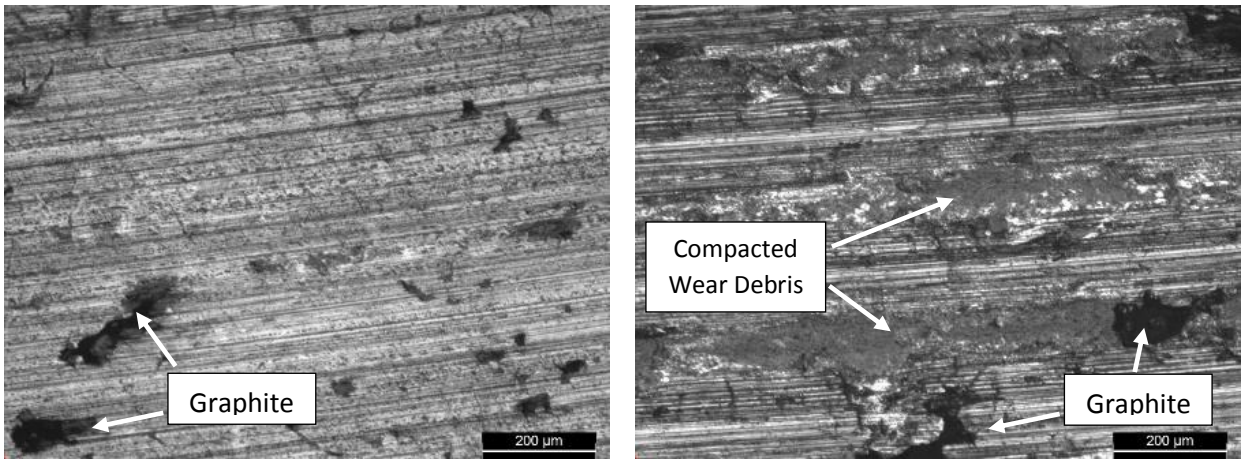

(a) (b)

Fig. 8: OM observations of the wear tracks of the discs tested at 30 kPa for the friction material 1 (a), 5 (b).

Element	**Friction material 1 [wt.%]**	**Friction material 2 [wt.%]**	**Friction material 3 [wt.%]**	**Friction material 4 [wt.%]**	**Friction material 5 [wt.%]**
Fe	73.9	67.0	55.0	35.2	14.5
Al	1.6	6.2	6.2	1.6	-
Mg	1.7	4.7	9.5	-	5.2
Cu	8.8	4.3	-	22.2	-
Sn	3.3	5.7	6.2	2.0	3.0
Zn	5.0	3.6	7.5	3.2	-
Ca	1.3	2.1	1.4	2.6	5.3
S	1.6	2.6	2.7	2.3	3.3
Cr	1.1	2.4	2.2	-	-
Si	1.7	1.4	9.3	1.8	3.4
Zr	-	-	-	18.8	35.5
Ti	-	-	-	7.4	23.3
Ba	-	-	-	3.1	6.5

Table 2: EDXS analysis on the secondary plateaus of the pins tested at 30 kPa.

To complete the picture, the static friction coefficient of worn and unworn friction materials were also evaluated and the results are plotted in Fig. 8. It can be noticed that the values of the static COF are comparable for the tests conducted starting both from the new and already worn friction material specimens. Moreover, the static friction seems not to be influenced by the contact pressure under the adopted experimental conditions. The experimental values are in between 0.20 and 0.25, i.e., much lower than the values of the kinetic COF.

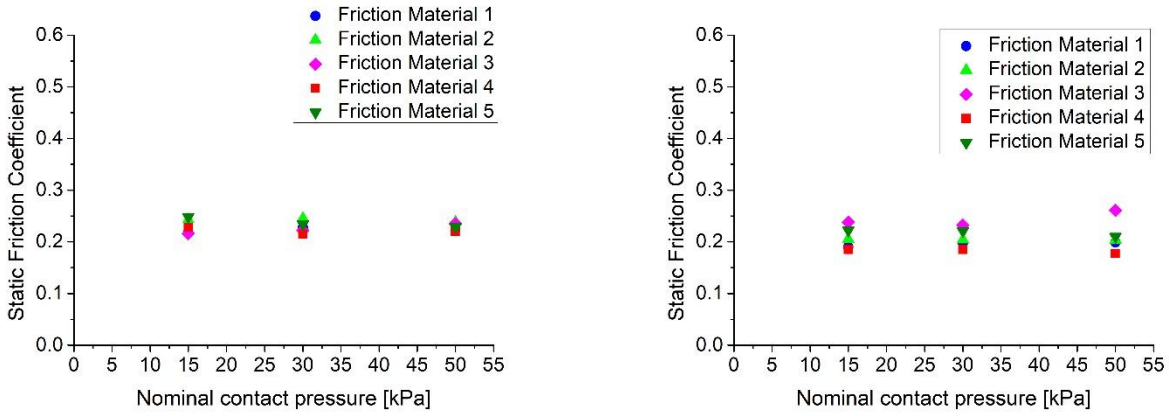

(a) (b)

Fig. 9: Static COF for the friction materials in (a) initially unworn (new) and (b) tested after preliminary wearing out (run-in conditions).

4. Discussion

The COF is given by the ratio of the tangential force, F_T, required to start the motion between two bodies in contact (static COF) or to maintain a given sliding velocity (kinetic COF), divided by the acting normal force, F_N. The tangential force, is given by the product of the mean shear stress, τ_m, required to separate the asperities in contact and the real area of contact, A_r [21, 22]. The COF can be thus expressed by the following relationship:

$$COF = \frac{\tau_m \cdot A_r}{F_N} \qquad 1.$$

In general, τ_m depends on the strength of the adhesive bonds forming at the contacting asperities. A contribution from the local plastic deformations, mainly due to the abrasive contribution, may be also present, if hard and angular particles are present at the contact regions [21, 23].

As concerns the static COF, quite surprisingly, the experimental values do not depend on the friction material, whether low-met or NAO, and also do not depend on the applied pressure, p (Fig. 8 a) and b)). They are also much lower than the kinetic COFs. The independence from the contact pressure, p, can be explained by considering that a decrease in p, i.e., a decrease in F_N, is accompanied by a corresponding decrease in the extension of the real area of contact A_r. A direct proportionality between A_r and F_N is reported for metals [21, 23, 24]. The same can be assumed to be valid also for the composite materials under present investigation. As reported, for example, by Eriksson and Jacobson [6], the real area of contact involves specific regions within the contact plateaus, and the actual extension of these regions is depending on the applied pressure. unless specific phenomena are triggered by pressure changes, like the thermal decomposition of particular constituents due to an excessive temperature rise [25]. However, this is not the case for the present study, and we argue that the ratio A_r/F_N does not greatly depend on p. From eq.1, it is then obtained that τ_m is mostly responsible for the static COF. This observation is coherent with the lower values of the static COF with respect to the kinetic ones, and explains also why static COFs have similar values independently from the friction material. In fact, the adhesive theory of friction assumes that τ_m depends on the work of adhesion, i.e., on the surface energies of the mating bodies [21, 26-28]. The surfaces of the contacting bodies are contaminated by atmospheric oxygen, water and other organic molecules [21, 26]. Oxygen produces the formation of a very thin layer of iron oxides on the cast iron surface [29]. Water and organic molecules are physically absorbed on the surfaces of both mating bodies and influence their surface energies, resulting in a sort of lubricating action [29, 30]. Therefore,

contaminants lead to a decrease in the surface energies and, thereby, in the work of adhesion. This determines low values of τ_m, that are also roughly independent from the specific composition of the friction material, since different composition of the composite materials are not such to induce significant differences in the surface absorbed layers, that is actually ruling the adhesive interactions between mating surfaces.

Regarding the kinetic COF, from the friction traces shown in Fig. 4. it can be clearly inferred that, at the onset of sliding, the COF is in the range 0.2-0.3, i.e., quite close to the values of the static COF. However, during the run-in stage the kinetic COF increases with time. Such an increase can be attributed to the progressive removal of the surface contaminants and consequent increase in the surface energies at the contacting asperities, leading to the formation of the contacting plateaus. These are the regions where the contact between the mating bodies is finally established [11]. According to the data in Table 2 and numerous literature investigations [9, 12, 13, 31], the secondary plateaus contain almost all of the ingredients of the friction materials, together with a large amount of Fe-oxides originating from the wear of the counterface cast iron disc (in general such oxides are a mixture of magnetite, hematite and wüstite, being magnetite generally prevailing [12]). Fig. 8 clearly shows that cast iron discs underwent abrasive wear with the formation of metallic debris, oxidized and partially transferred onto the pin worn surface. This process has been described in several similar systems, like in ceramic reinforced Al- or Cu-based composites dry sliding against a steel counterface [32-34]. The hard reinforcements are reported to cut and abrade the counterface and promote material transfer. Therefore, Fe-oxide rich tribolayers would form on the worn surfaces of the composites. The run-in stage is quite prolonged for low-met materials (Fig, 4a), because of the relatively high content of abrasive particles. These components of the friction material render the tribological interactions quite intense, influencing also the dynamics of formation of extended Fe-oxide rich secondary plateaus (Fig. 4), that in fact requires longer times.

Once a stable dynamic friction layer is established, COF is mainly determined by its characteristics and in particular of the secondary plateaus, which determine the intensity of the adhesive interactions between the contacting surfaces. Fig. 10 is quite revealing in this respect. Here the experimental values of the kinetic COF obtained at 30 kPa, are plotted as a function of the Fe content in the secondary plateaus listed in Table 2 (similar trends are obtained using the results for the other contact pressures). It can be seen that the kinetic COF increases with the amount of Fe in the secondary plateaus, i.e., with the amount of Fe-oxides. Considering that the Ar/F_N ratio can be also in this case assumed to be roughly independent from the contact pressure, the experimental trend can be explained by considering the dependence of τ_m on the work of adhesion. The increase in the content of Fe-oxides in the secondary plateaus induces an increase in the work of adhesion, and therefore in τ_m due to the raise in the tribological compatibility of the mating surfaces, since the counterface is made by cast iron [21, 26, 28]. In case of steel-steel contact, corresponding to 100 wt.% Fe in the plot in Fig. 10, the friction coefficient is reported to be in the 0.6-0.8 range [14, 16]. A typical value of 0.7 is then included in the graph in order to have an approximate reference when the mating materials are fully made by Fe-oxides. These results show that the kinetic COF is mainly dependent on the fraction of Fe-oxides present in the secondary plateaus. Of course, as seen in the Introduction other components originating from the friction material may affect the COF by influencing the work adhesion, but the present results indicate the Fe-oxides may play a predominating role. In low-met friction materials 1 and 2, the kinetic COF is higher because of the larger amount of Fe-oxides, whose formation is favored by the presence of the ceramic abrasives, able to remove more efficiently the surface oxides forming on the cast iron counterface. On the contrary, in NAO materials this mechanism is not that effective for their lower concentration of abrasives. As a consequence, a lower amount of Fe-oxides is formed and then embedded into the secondary plateaus, resulting in a lower value of τ_m (and thus of COF). It also seems that when the weight % of Fe is below 50%, τ_m is not so influenced by the Fe-oxides, but rather by the interaction with other constituents of the friction layers. In order to clarify better this point, additional tests with other different friction materials and in different conditions are required.

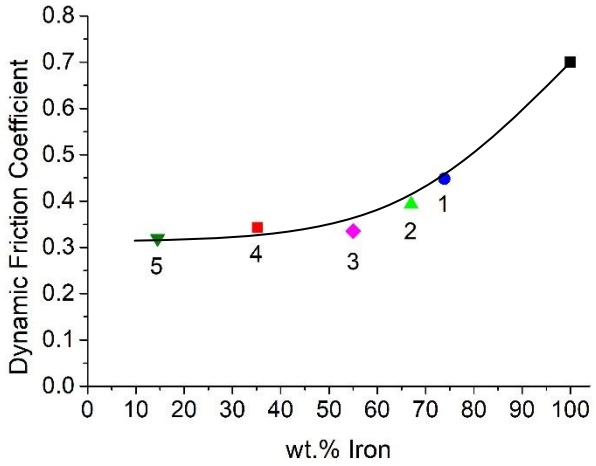

Fig. 10: Dynamic friction coefficient as a function of the wt.% of iron detected inside the secondary plateaus. The COF for 100 wt.% Fe datum is taken from literature data [14, 16] (the numbers in the graph indicate the materials under study).

The friction coefficient curve depicted in Fig. 9, was fitted by means of the following exponential relationship:

$$\mu = e^{(a+b\,x+c\,x^2)} \qquad 2.$$

where μ is the dynamic friction coefficient and x is wt.% of iron detected in the secondary plateaus. The fitting parameters are reported in Table 3.

a [-]	b [1/wt.%]	c [1/(wt%^{2})]	Adj. R-Square
-1.0268	-0.00863	1.5330 10^{-4}	0.98

Table 3: Exponential-fitting parameters for eq. 2.

5. Conclusions

The kinetic and static COFs were determined for 5 commercial low-met and NAO friction materials dry sliding against a grey cast iron counterface at low contact pressures. The main results can be summarized as follows:

1. The static COFs were found to be all in the range 0.18-0.25 irrespective of the materials and testing conditions.
2. The kinetic COFs were found to be higher for the low-met materials with respect to the NAO materials; in addition, longer run-in stages were recorded for the low-met materials.
3. The kinetic COFs were found to be independent from the contact pressure, i.e., they did not display the desired decrease as contact pressure was decreased.
4. The obtained results were explained in the frame of the adhesive theory of friction and considering the observed wear mechanisms.
5. The independence of the static COF from materials and operating conditions was attributed to the presence of contaminants on the surfaces, that reduced the surface energies and therefore the work of adhesion between the mating surfaces.

6. The kinetic COFs were justified by considering the Fe-oxide content in the friction layers (and, in particular, in the secondary plateaus) that play a prevailing role in determining the work of adhesion, given their high compatibility with the cast iron counterface.
7. The presence of a high amount of abrasives in low-met friction materials induces a longer run-in stage and thus the formation of secondary plateaus containing an increased amount of Fe-oxides originating from the tribo-oxidation of the counterface disc.
8. Different contact conditions deserve further investigations, with particular regard to the possible effects of the sliding velocity.

Acknowledgements
The Authors wish to thank Daniel Belluco and Elia Visintainer for the experimental support.

References

[1] A.E. Anderson, Friction and wear of automotive brakes, ASM Hndb. 18 (1992) 569-577.
[2] A. Day, Braking of Road Vehicles, Elsevier, Amsetrdam (2014).
[3] K. Bode, T. Schramm, N. Perzborn, S. Raczek, J. Munchoff, G.P. Ostermeyer, Low μ at low pressure – potential for reducing residual drag? In: Proceedings of Eurobrake, Lille, France, 13-15 may 2014.
[4] B. Breur, K.H. Bill, Brake Technology Handbook, SAE International; Pennsylvania, Warrendale, PA, 2008.
[5] P. Filip, L. Kovarik, M.A. Wright, Automotive Brake Lining Characterization (N. 973024). SAE Technical Paper, 1997.
[6] M. Eriksson, S. Jacobson, Tribological surfaces of organic brake pads, Tribol. Int. 33 (2000) 817-827.
[7] W. Osterle, M. Griepentrog, T. Gross, I. Urban, Chemical and microstructural changes induced by friction and wear brakes, Wear (2001), 1469-1476.
[8] G.P. Ostermayer, M. Muller, Dynamic interaction of friction and surface topography in brake systems, Tribol Int, 39 (2006) 370-380.
[9] P. Chandra Verma, L. Menapace, A. Bonfanti, R. Ciudin, S. Gialanella, G. Straffelini, Braking pad-disc system: Wear mechanisms and formation of wear fragments, Wear 322-323 (2015) 251-258.
[10] M.H. Cho, K.H. Cho, S.J. Kim, D.H. Kim, H. Jang, The role of transfer layers on friction characteristics in the sliding interface between friction materials against gray iron brake disks, Tribology Letters 20 (2005) 101-108.
[11] P.J. Blau, On the nature of running-in, Trib. Int. 38 (2005) 1007-1012.
[12] W. Österle, A.I. Dmitriev, The Role of Solid Lubricants for Brake Friction Materials, Lubricants, 4 (2016) doi: 10.3390/lubricants4010005.
[13] P.W. Lee, P. Filip, Friction and wear of Cu-free and Sb-free environmental friendly automotive brake materials, Wear (2013) 1404-1413.
[14] W. Österle, I. Dörfel, C.Prietzel, H. Roocha, A.L. Cristol-Bulthéb, G. Degallaix, Y.Desplanques, A comprehensive microscopic study of third body formation at the interface between a brake pad and brake disc during the final stage of a pin-on-disc test. Wear 267 (2009) 781–788.
[15] W. Österle, A.I. Dmitriev, H. Kloß, Possible impacts of third body nanostructure on friction performance during dry sliding determined by computer simulation based on the method of movable cellular automata, Tribology International 48 (2012) 128–136.
[16] G. Straffelini, D. Trabucco, A. Molinari, Oxidative wear of heat-treated steels, Wear 250 (2001) 485-491.
[17] S.F. Scieska, A. Jankowski, The importance of Static Friction Characteristics of Brake Friction Couple, and Methods of Testing, Tribotest journal, 3 (1996) 137-148.

[18] A.R. Rihai, A.T. Alpas, Wear map for grey cast iron, Wear 255 (2003) 401-409.
[19] G. Straffelini, M. Pellizzari, L. Maines, effect of sliding speed and contact pressure on the oxidative wear of austempered ductile iron, Wear 270 (2001) 714-719.
[20] G. Straffelini, P. Chandra Verma, I. Metinoz, R. Ciudin, G. Perricone, S. Gialanella, Wear behavior of low metallic friction material dry sliding against a cast iron disc: Role of the heat-treatment of the disc, Wear 348-349 (2016) 10-16.
[21] E. Rabinowicz, Friction and wear of materials, 2nd ed., Wiley (1995).
[22] I.M. Hutchings, Tribology, Edward Arnold Publishers, London, 1992.
[23] G. Straffelini, A simplified approach to the adhesive theory of friction, Wear 249 (2001) 78-84.
[24] S.C. Lim, M.F. Ashby, Wear mechanisms maps, Acta mater. 35 (1987) 1-24.
[25] X. Xiao, Y. Yin, J. Bao, L. Lu, X. Feng, Review on the friction and war of brake materials, Advances in Mechanical Engineering 8 (2016) 1-10.
[26] B. Bushan, Introduction to tribology, John Wiley & Sons, 2013.
[27] K. Miyoshi, Solid Lubrication, Fundamentals and Applications, Marcel Dekker, 2001.
[28] G. Straffelini, Friction and wear, Methodologies for Design and Control, Springer Verlag, 2015.
[29] G. W. Stachowiak, A.W. Batchelor, Engineering Tribology, Tribology Series 24, Elsevier, Amsterdam, 1993.
[30] S. Mirzababaei, P. Filip, Impact of humidity on wear of automotive friction materials, Wear 376-377 (2017) 717-726.
[31] J. Kukutschova, V. Roubicek, M. Maslan, D. Jancik, V. Slovak, K. Malachova, Z. Pavlickova, P. Filip, Wear performance and wear debris of semimetallic automotive brake materials, Wear 268 (2010) 86–93.
[32] Y.Z. Zhan, G. Zhang, Mechanical mixing and wear-debris formation in the dry sliding wear of copper matrix composite, Tribology Letters 17 (2004) 581-592.
[33] W. Ames, A.T. Alpas, Effect of microstructure and counterface material on the sliding wear resistance of particulate reinforced aluminum matrix composites, Metall. Mater. Trans., 7A (1994) 969-983.
[34] G. Straffelini, Experimental observations of subsurface damage and oxidative wear in Al-based metal matrix-composites, Wear 245 (2000) 216-222.